JOURNAL OF MATERIALS SCIENCE 25 (1990) 4125–4132

Cavitation and fracture of mechanically alloyed aluminium at high homologous temperatures

T. R. BIELER*, G. R. GOTO, A. K. MUKHERJEE
University of California, Davis, Department of Mechanical Engineering, Division of Materials Science and Engineering, Davis, California 95616, USA

The tensile behaviour of mechanically alloyed (dispersion strengthened) IN90211 was characterized at strain rates between 0.0001 and 340 sec^{-1} at temperatures between 425 and 475° C. At strain rates above 0.1 sec^{-1}, superplastic elongations were obtained (maximum elongation 525% at 475° C, 2.5 sec^{-1}). Large elongations were possible due to the lack of cavitation, even though the strain-rate sensitivity was lower ($m \approx 0.25$) than usually found in superplasticity. Cavitation was precluded by the morphology of the platelet-shaped grains in which low-angle subgrain boundaries were predominantly perpendicular to the tensile axis. Grain-boundary sliding was observed along high-angle grain boundaries which were generally parallel to the tensile axis. At the high homologous testing temperatures (0.76 to 0.81), concurrent grain-boundary sliding and lattice slip was made possible by the rapid lattice diffusivity and easy climb of lattice dislocations over dispersions in the matrix and grain boundaries.

1. Introduction

Cavitation that leads to fracture is a major concern for the practical use of materials for elevated temperature service under creep conditions, and also for superplastic forming. Creep rupture life has been extended by thermo-mechanical processing in order to obtain elongated grains so as to minimize the grain-boundary area perpendicular to the tensile direction [1, 2]. Superplasticity is possible under certain conditions when the alloy has a fine, equiaxed grain size. Many superplastic alloys cavitate severely during deformation [3]. Methods that reduce or prevent cavitation have been developed, such as superposed hydrostatic pressure [4, 5]. In addition, cavitation is minimal in two-phase alloys where grains of the two phases have a different hardness (e.g. α-βTi, Pb–Sn, and Al–Zn). The role of deformation mechanisms, grain-boundary morphology, and diffusion are investigated to determine their role in cavitation and fracture of IN90211 (or the lack thereof).

IN90211 is a mechanically alloyed aluminium alloy that has a composition similar to 2124 aluminium alloys. In addition to the solution hardening provided by magnesium atoms and the precipitation hardening provided by copper in the form of θ phase, the mechanical alloying process introduces fine oxide and carbide dispersions [6, 7]. The presence of these dispersions places this alloy in the class of metal matrix composites. IN90211 is nominally the same as IN9021 as described in the literature [8–11], but it is slightly richer in alloying elements (Table I).

2. Experimental procedure and results

Tensile specimens were made from processed sheet material produced by Inco MAP Light Alloys, Huntington, West Virginia and subsequently processed at the Research and Development Division of Lockheed Missiles and Space Co., Inc. Two lots of material were used, IN9021 sheet, and IN90211 extruded rod. The extruded rod was forge flattened and warm rolled to sheet 2.5 mm thick, annealed, and water quenched. The IN90211 specimens used for superplasticity had a gauge length of 6.3 mm, and were nominally 2.5 mm square. Longer specimens (51 mm) that were used for creep experiments were made from 2 mm IN9021 sheet, whose processing history was similar. Marks were made along the tensile axis with a pencil and photographed before and after deformation to permit accurate local strain and area reduction measurements. Local strain was found to agree with the correlation between the reduction of area, RA, and engineering strain, ε: $RA = (A_0 - A)/A_0 = \varepsilon/(1 + \varepsilon)$. It was noted that more strain occurred in the thickness direction than in the width direction, as the area reduced. The overall stress–strain rate behaviour was typical for superplasticity, exhibiting three deformation regimes, with maximum elongations occurring where the strain rate sensitivity is highest, in the middle regime. This regime occurred between strain rates of 0.1 and 100 sec^{-1}, at homologous temperatures between 0.76 and 0.81. The tensile test results are described in detail elsewhere [12, 13].

Cavitation was investigated with optical microscopy, using the polished cross-section of the fractured specimen that included the fracture surface and the unstrained shoulder of the specimen. The width of the specimen where void density was measured was compared with the photographs of the deformed specimen

Present address: Department of Metallurgy, Mechanics, and Materials Science, Michigan State University, E. Lansing, Michigan 48824-1226.

0022–2461/90 $03.00 + .12

TABLE I Composition (wt %) of IN9021 and IN90211

	Mg	Cu	C	O	Al_2Cu	Al_4C_3	Al_2O_3	Al
IN9021	1.5	4.0	1.1	0.8				
IN90211	2.0	4.4	1.1	0.8				91.7
	2.0*	0.9*			6.4*	4.3*	1.7*	84.7*
					4.1 vol %*	4.1 vol %*	1.2 vol %*	90.6 vol %*

*Assuming 80% Cu in Al_2Cu, O and C in Al_4C_3, Al_2O_3, and Mg in solution.

to determine the reduction of area corresponding with the region where cavity density was measured. At each location along the tensile axis three or four micrographs were taken. Cavity density measurements were generally made 100 and 450 μm from the fracture surface along the tensile axis, although measurements were also made at greater distances in some specimens (Fig. 1 and Table II).

Cavitation in IN90211 was found to be less than 4% in the vicinity of fracture in the tensile specimens. Cavity density was normalized by subtraction of the porosity in the shoulder of each specimen. The shoulder porosity varied considerably, from 0.01 to 2.4%, (counting voids larger than 1 μm), as specimen to specimen variation resulted from the fact that the rolled sheet was originally an extruded rod. Extremely fine features appearing as pin holes (of the order of 0.5 μm) were observed on many micrographs. If these are cavities, they are populous in some specimens, providing as much as an additional 5% void fraction. Because these are of the order of the grain size, it is possible that they are grains pulled out during the polishing process, and not associated with cavitation.

Bar charts and micrographs showing the distribution of cavities are shown in Fig. 1. The distribution of cavities observed in specimens deformed at a high strain rate differed from that at low rates, as illustrated in Fig. 1c to e. At the higher rate (75 sec^{-1}), the cavity-size distribution was characterized by numerous small cavities, with the largest contribution to the total cavity volume coming from cavities smaller than 5 μm. At the lower rates (e.g. 0.0001 sec^{-1}), the majority of the cavity volume came from cavities greater than 5 μm (Table II).

Cavity density varied with temperature and strain rate. Cavitation is plotted as a function of true strain

TABLE II Cavitation as a function of strain and strain rate

Conditions			Distance from fracture surface (μm)	Cavity diameter (μm), Number, and Area (μm^2)										Cavity density (%)
°C sec^{-1} Area (μm^3) measured	Strain RA %	True strain		1–2.5		2.5–5		5–7.5		7.5–10		> 10		
				No.	area	No.	area	No.	area	No.	area	No.	area	
425 0.0001			–	–	–	–	–	–	–	–	–	–	–	–
37620	66	1.1	100	17	41	13	144	9	276	3	120	1	99	1.81
	59	0.9	450	10	24	10	110	1	31	1	0	0	0	0.44
	Undef.			0	0	0	0	0	0	1	60	0	0	0.16
1.000			–	–	–	–	–	–	–	–	–	–	–	–
28215	98.8	4.4	100	9	7	7	77	3	92	0	0	0	0	0.63
	98.2	4.0	450	24	43	9	99	0	0	0	0	0	0	0.51
	Undef.			6	14	0	0	0	0	0	0	0	0	0.05
75			–	–	–	–	–	–	–	–	–	–	–	–
37620	87	2.0	100	23	24	10	110	3	92	0	0	0	0	0.60
	83	1.8	450	15	5	2	22	0	0	0	0	0	0	0.07
	Undef.			13	31	0	0	0	0	0	0	0	0	0.08
330			–	–	–	–	–	–	–	–	–	–	–	–
35380	74	1.3	100	391	137	15	121	3	153	0	0	0	0	1.16
	67	1.1	450	296	−91	8	44	2	61	0	0	0	0	0.04
	Undef.			334	803	4	44	0	0	0	0	0	–	2.40
475 1×10^{-6}			–	–	–	–	–	–	–	–	–	–	–	–
26535	2.7	0.03		147	296	0	0	0	0	0	0	0	0	1.12
	Undef.			24	58	0	0	0	0	0	0	0	0	0.22
0.001				–	–	–	–	–	–	–	–	–	–	–
37620	73	1.3	100	20	10	8	66	8	245	7	421	4	552	3.44
	70	1.2	450	19	7	9	77	3	92	1	60	0	0	0.63
	Undef.			16	38	2	22	0	0	0	0	0	0	0.16
2.5			–	–	–	–	–	–	–	–	–	–	–	–
26535	96.7	3.4	1000	93	31	0	0	0	0	0	0	0	0	3.44
	Undef.			80	192	0	0	0	0	0	0	0	0	0.73
75			–	–	–	–	–	–	–	–	–	–	–	–
37620	93.3	2.71	100	91	216	28	309	14	430	0	0	3	298	3.33
	93.2	2.69	450	94	219	23	254	11	337	6	361	0	0	3.11
	93.2	2.69	800	91	212	17	188	13	399	0	0	0	0	2.12
	91.9	2.52	2770	180	428	17	141	13	44	0	85	0	0	1.86
	Undef.			3	7	0	0	0	00	0	0	0	0	0.02
330			–	–	–	–	–	–	–	–	–	–	–	–
35380	72	1.3	100	193	48	3	0	0	0	0	0	0	0	0.14
	69	1.2	450	185	29	2	−11	0	0	0	0	0	0	0.05
	Undef.			173	413	3	33	0	0	0	0	0	0	1.27

in Fig. 2. (The relationship between true strain and area reduction was used to estimate the true strain near the fracture.) The maximum cavity densities of 3% to 4% were found at the fracture surfaces in specimens deformed above and below the optimum superplastic strain rate at 475° C. The smallest cavity densities were found at the optimum superplastic strain rates between 1 and 2.5 sec^{-1}. (The maximum elongation of 525% occurred at 475° C and 2.5 sec^{-1}.) The 425 and 475° C specimens with optimum elongation fractured at the same area reduction of 98.8%. The cavitation in the 475° C specimen was lower, as indicated in Fig. 2, although the fracture surface was lost due to excessive grinding. Cavitation generally increased with temperature away from optimum superplastic conditions, but decreased with temperature in the optimum superplastic regime.

Grain morphology was determined from transmission electron microscopy (TEM) observations. TEM specimens were prepared by grinding 3 mm punched discs to 0.2 mm, and electrolytic thinning at −20° C in a 1:3 ratio of nitric acid and methanol. Specimens were taken both parallel and perpendicular to the rolling plane. Grains were found to be nominally disc shaped in accordance with the rolling plane, about 2 to 3 μm diameter and about 0.3 μm thick (Fig. 3). Grains consisted of many submicrometre subgrains, where subgrain walls were usually perpendicular to the rolling plane. Subgrain walls were low angle, but exceptionally stable, because they were particles arising from the mechanical alloying process. The boundaries between platelets were typically high-angle grain boundaries. These features were similar to observations on IN9052, another mechanically alloyed aluminium where the microstructure was described as having submicrometre subgrains [14]. These observations apply both to undeformed and deformed specimens, indicating the exceptional stability of the grain size during deformation.

Grain-boundary sliding and fractography were investigated using scanning electron microscopy (SEM). Some SEM specimens were coated with gold–palladium to improve resolution. Grain-boundary sliding was observed on pre-polished surfaces of tensile specimens deformed superplastically. At lower superplastic strain rates (1 to 5 sec^{-1}), the sliding entities were typically 2 to 3 μm platelets, but at

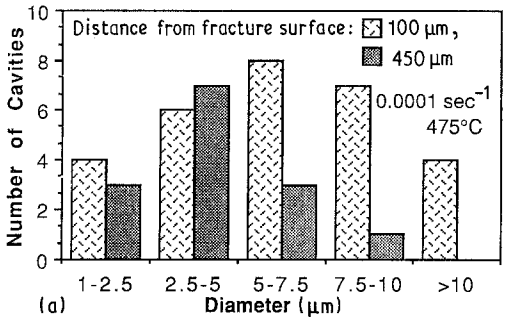

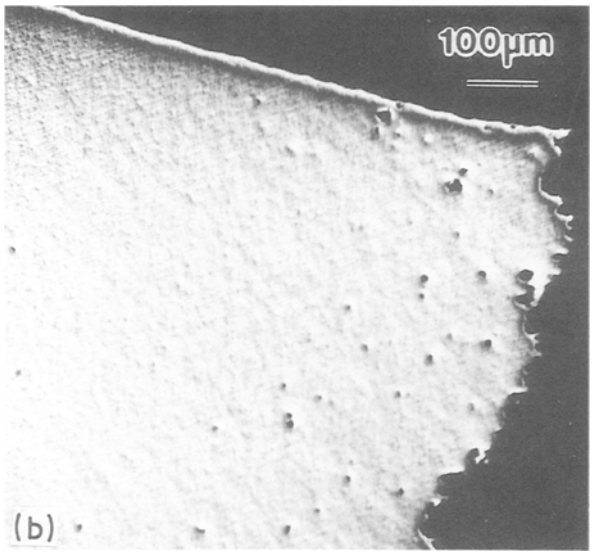

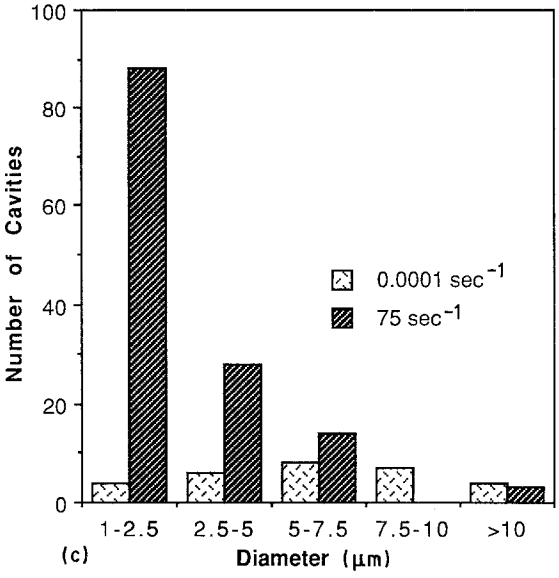

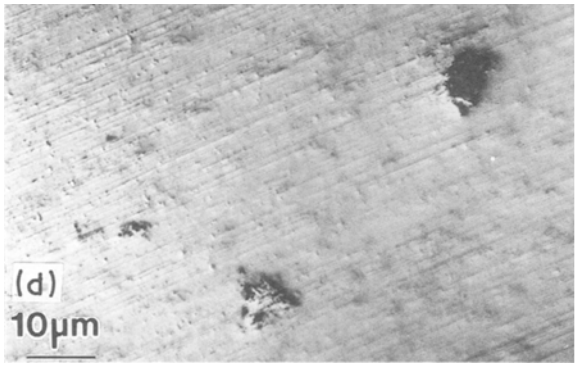

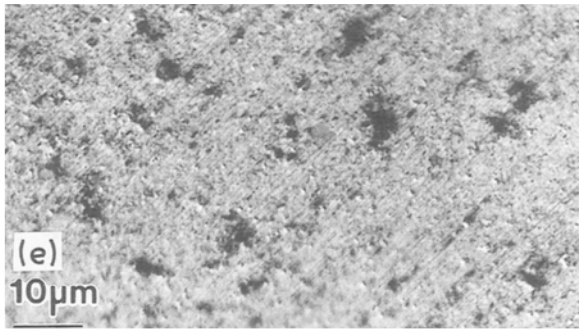

Figure 1 (a) The distribution of cavities near the fracture surface (as shown in the micrograph, (b)) of a specimen deformed at 475° C, 0.0001 sec^{-1}. (c) The cavity density of 3% near the fracture surface is the same for two specimens deformed at strain rates of 0.0001 (d) and 75 sec^{-1} (e), but the size distribution is different.

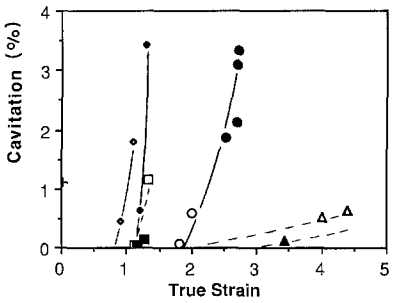

Figure 2 Cavity density (%) is plotted as a function of true strain (determined from reduction of area) for specimens deformed at (◇, △, ○, □) 425 and (+, ◆, ▲, ●, ■) 475° C. (◇) 1×10^{-4} sec^{-1}, (△) 1 sec^{-1}, (○) 75 sec^{-1}, (□) 330 sec^{-1}, (+) 1×10^{-6} sec^{-1}, (◆) 1×10^{-4} sec^{-1}, (▲) 2.5 sec^{-1}, (●) 75 sec^{-1}, (■) 330 sec^{-1}.

higher strain rates, individual subgrain features were predominant (Fig. 4). At strain rates below the superplastic regime, fracture surfaces exhibited an overall ductile-dimple mode, with intergranular fracture features on the surfaces of the dimples (Figs 5a and b). The dimple size and spacing correlated well with observed cavities in the optical micrographs, indicating that cavity growth and inter-linkage preceded failure of low strain rate specimens. Fracture surfaces of superplastic specimens in Fig. 5c exhibited intergranular fracture. Fracture surfaces of extremely high strain-rate (330/sec) specimens above the superplastic regime, (Fig. 5d), were similar to that of the low strain-rate regime, but with fewer granular features observed on the dimple surfaces and a smaller cavity spacing of 3 to 5 μm.

X-ray diffraction was done on an undeformed specimen and compared with a superplastically deformed specimen [12]. The specimens were oriented such that the moving X-ray beam was perpendicular to the tensile axis. The results from the analysis are two-fold, and tabulated in Table III; *d*-spacings were smaller than standard pure aluminium powder samples, and the texture present in the undeformed specimen increased as a result of superplastic deformation. The smaller *d*-spacings resulted from the residual compressive stresses developed around the oxide and carbide particles during cooling. The texture of the undeformed specimen was indicated by the relative intensity of {2 0 0} planes, which was 1.3 times higher in the undeformed sample compared to the aluminium powder standard. This preferred orientation of {0 0 1} poles parallel to the rolling direction increases the number of {1 1 1} slip planes oriented along the planes of maximum shear stress. The superplastically deformed {2 0 0} peak intensity was twice the Al {2 0 0} powder standard, indicating that the superplastic deformation increased the texture already present. This observation was unexpected as superplastic deformation often results in a decrease in texture due to the sliding and rotation of the grains.

3. Discussion

3.1. Deformation mechanisms

An analysis of the IN9021(1) data indicated that the deformation mechanisms responsible for the superplastic deformation of IN9021 are both an $n = 3$ slip mechanism in the grains and an $n = 2$ grain-boundary sliding mechanism [12]. The homologous temperature is high enough for lattice diffusivity to be dominant, permitting relatively facile climb of dislocations over dispersions in the matrix. The threshold stresses associated with these particles are small, because diffusivity is high. Concurrently, the presence of magnesium in the matrix limits dislocation progress by solute-drag. The lattice dislocations become extrinsic grain-boundary dislocations when they reach the boundary, permitting grain-boundary sliding. However, though all these processes occur, they do so in sequence, and the rate-limiting step is dislocation glide in the interior of the grains.

The sliding of platelet-shaped clusters cause features similar to the inverted hour-glass shape described by the transitional core–mantle model of Mayo and Nix [15]. This model assumes that the deformation mechanism dominant in the interior (core) is different from the dominant mechanism near the grain boundary (mantle). Superplasticity results as a transition between the stresses where the core and mantle mechanisms occur in parallel, independent of each other, contrary to the result of the above analysis. The core–mantle model requires a low dislocation density in the grain interior compared to the boundary, but the high dislocation density in the IN90211 grains ($> 4 \times 10^{13}$ m^{-2}) makes the model difficult to apply to IN9021. Therefore, if the above analysis is correct, then the inverted hour-glass morphology of the observed grain-boundary sliding does not imply that the core–mantle model accounts for the deformation mechanism. Mayo's core–mantle model was developed using two-phase eutectic materials, while the IN90211 is a quasi-single phase material.

3.2. Grain morphology

The shapes of grains in extruded oxide dispersion strengthened (ODS) aluminium alloys has been investigated by Tweed *et al.* [16]. In an extruded ODS Al/Al_2O_3 alloy, about half of the boundaries were found to be low angle. A high percentage (80%) of the

TABLE III X-ray diffraction of IN90211

(*hkl*)	Al*		IN90211 Undeformed			IN90211 Deformed 2.5 sec^{-1}, 475° C		
	d(nm)	I/I_0	*d*(nm)	I/I_0	I/I_{Al}	*d*(nm)	I/I_0	I/I_{Al}
(1 1 1)	0.2338	1.0	0.2331	1.0	1.0	0.2333	0.96	0.96
(2 0 0)	0.2024	0.47	0.2020	0.61	1.3	0.2021	1.0	2.1
(2 2 0)	0.1431	0.22	0.1430	0.29	1.3	0.1431	0.31	1.4
(3 1 1)	0.1221	0.24	0.1220	0.34	1.4	0.1221	0.47	2.0
(2 2 2)	0.1169	0.07	0.1168	0.08	1.1	0.1169	0.11	1.6

*Joint Committee on Powder Diffraction Standards, card number 4–787

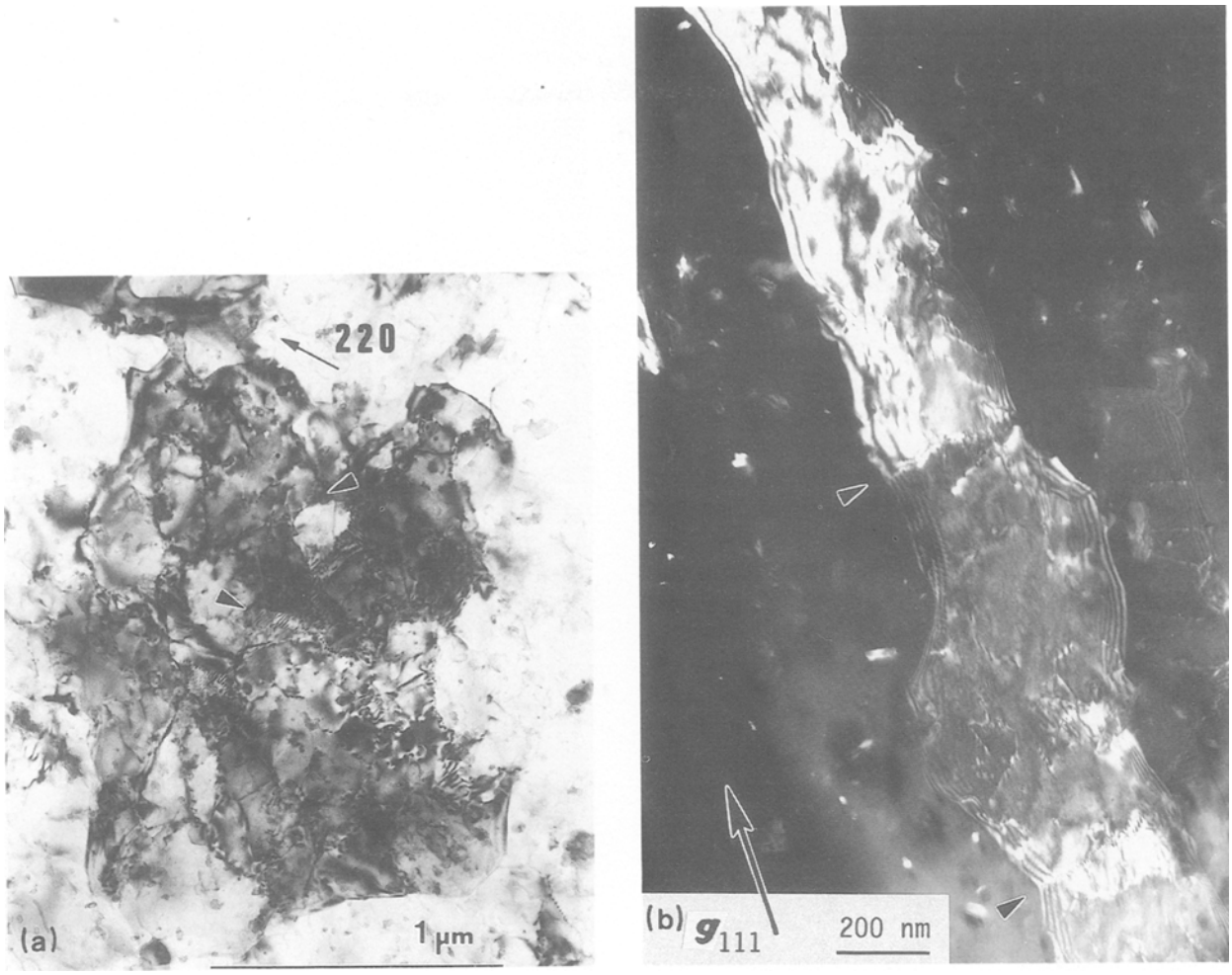

Figure 3 TEM images of a specimen deformed at 475° C, 10 MPa, for 2.7×10^6 sec to a strain of 0.03. Grain morphology shows platelet shaped cluster of subgrains with low-angle boundaries (arrows). (a) Bright-field image with 0 0 1 pole parallel to beam, rolling plane parallel to page. (b) Dark-field image (1 1 1 spot) with rolling plane perpendicular to page, particles pin subgrain boundaries. Dislocation density in middle grain was greater than $4 \times 10^{13} m^{-2}$.

low-angle boundaries were perpendicular to the extrusion/drawing direction, and similarly, 80% of the high-angle boundaries were parallel to the extrusion and drawing direction. Particles were found to pin the high-angle boundaries in agreement with the Zener estimate. However, particles were found to pin low-angle boundaries more effectively than high-angle boundaries. They indicated that low-angle boundaries have about 1/5 of the energy of high-angle boundaries. The observations can be rationalized using the lower

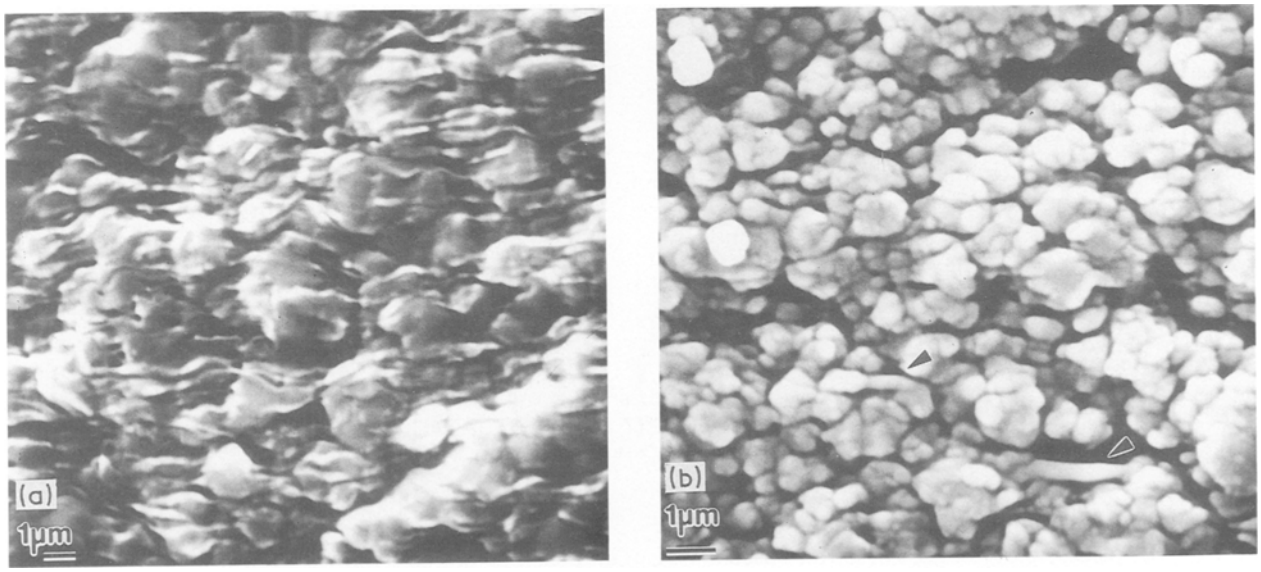

Figure 4 The degree of grain-boundary sliding depends upon the applied stress. (a) Grain-cluster sliding at low stress and 1 sec^{-1} strain rate (local strain of 1.8), sliding of clusters appears similar to "the inverted hour-glass" predicted by the core–mantle theory of Mayo. (b) Individual (sub)grains at higher stress and 75 sec^{-1} (local strain of 2.7). Arrows indicate whisker-like features discussed in text.

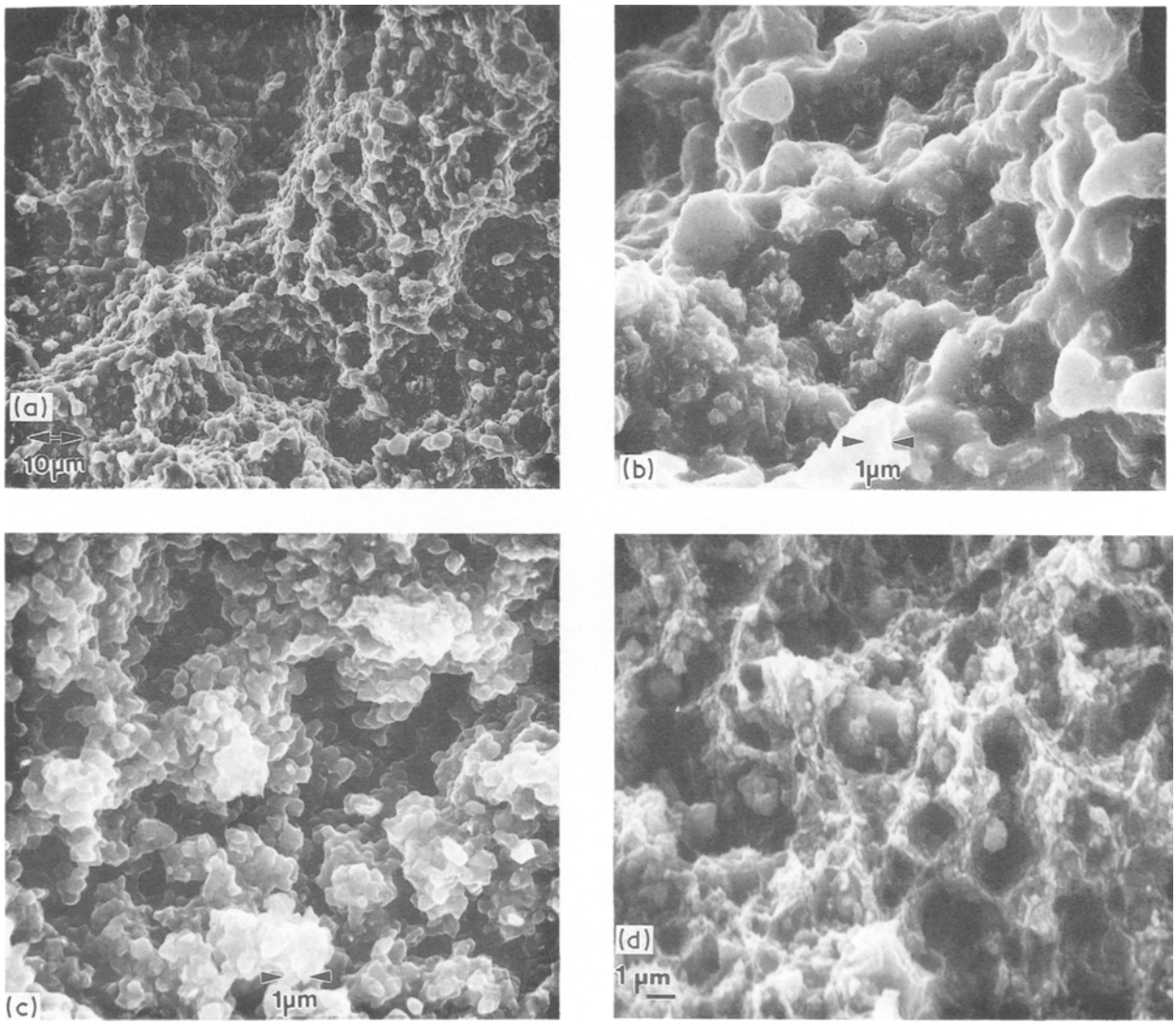

Figure 5 Fracture surfaces of deformed specimens. (a, b) 475° C at 0.0001 sec^{-1}, (c) 475° C at 75 sec^{-1} (high superplastic), (d) 425° C at 330 sec^{-1}.

low-angle boundary energy in the Zener estimate, which provided correlation with the observations. In addition, low-angle boundaries were more stable than high-angle boundaries.

The above description also applies to the trend of grain boundaries in IN9021(1), although no quantitative measurements were made. Numerous low-angle boundaries were clearly observed in the IN9021 specimen viewed in TEM perpendicular to the rolling direction (Fig. 3). The grains generally had high-angle boundaries along the platelet surface interfaces, while the sub-boundaries within the grains were usually low angle. Grain-boundary clusters were observed to slide and rotate in IN9021 at the optimum strain rates. The number of individual grain entities observed increased (and clusters decreased) in the specimen deformed at higher stress and strain rate (Fig. 4). The higher stress apparently activated sliding on boundaries that were stable at a lower stress and strain rate.

A low cavity nucleation rate in IN90211 is consistent with its grain morphology. Creep in nickel-based alloys has been reduced when the number of boundaries oriented perpendicular to the tensile axis is minimized by making grains columnar [1, 2]. IN9021 has some features of columnar grains in that the majority of the grain-boundary surface perpendicular to the tensile axis consists of low-angle boundaries, which resist cavity nucleation and sliding much more effectively than high-angle boundaries. When these boundaries are subjected to a high enough stress to start sliding, more damage is done, increasing the nucleation sites for cavities (Figs 1c and e).

The increase in texture differs from the usual expectation in superplasticity, i.e. an increase in the randomness of grain orientation by the sliding and rotation of grains. The grain-boundary sliding in IN9021 is different from that in usual superplastic materials since the grain aspect ratio is not equiaxed (Fig. 6). Because sliding in a direction perpendicular to the plane of the grain is difficult (due to the low-angle boundaries) the grains remain in the same plane as they started. This accounts for the lack of a decrease in texture, but not the observed increase. This increase in texture must result from grains rotating within their planes to align themselves in the direction where {1 1 1} planes are aligned more favourably for slip. Consequently, the grains must become thinner and/or more elongated with strain. The surface in Fig. 4 clearly shows small rotations, and the appearance

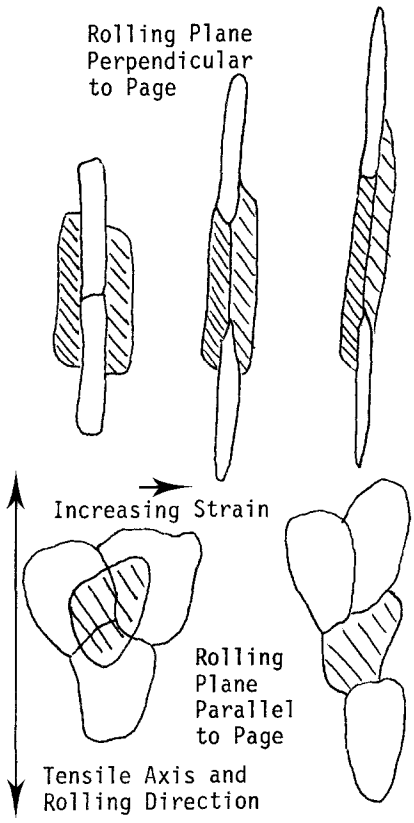

Figure 6 Schematic diagram showing sliding of platelet-shaped grains during superplastic elongation.

of inverted hour-glass shapes is consistent with elongation of grains along the tensile axis. Therefore, slip in the grains must occur during superplastic deformation. Slip can then help accommodate (in addition to diffusion) the compatibility problems at triple points and obstacles, and thus help preclude cavitation.

3.3. Mechanism of cavitation

Cavitation is minimized at optimum superplastic strain rates, unlike the results of other alloys [3]. Cavitation generally increases with grain-boundary dislocation activity and grain size when grain-boundary sliding is the rate-controlling mechanism. In IN9021(1), grain-boundary sliding is not rate limiting. The resistance to dislocation glide limits the rate of production of extrinsic grain-boundary dislocations, which in turn limits the rate of sliding. When sliding causes incompatibilities at triple points, particles or ledges in the boundary, stress concentrations can be accommodated by slip in the adjacent grain. When stress concentrations can be easily accommodated, cavitation is precluded. Furthermore, the vacancies that usually end up in cavities within the grain boundary, in the case of a diffusion-limited growth process, are in competition with the abundant cavity sources and sinks in the numerous particle interfaces and the large number of dislocations.

With increasing temperature, the mobility of vacancies increases, so cavities that do start growing can attract vacancies and grow faster with increasing temperature. This was evident in the large average cavity size near the fracture surface in the specimen strained at 0.0001 sec^{-1} at 475° C (Fig. 1), where more than 1 h elapsed before fracture. A similar volume of cavitation was seen at the high end of the superplastic regime in the specimen deformed at 75 sec^{-1} where fracture occurred shortly after 0.05 sec. Cavities were smaller but more populous in the sample strained at high strain rate, where they had less time to grow by diffusive processes. However, due to the higher stress more nucleation sites were generated.

3.4. Fracture surfaces

The fracture surfaces of low strain rate, non-superplastically deformed specimens showed cavitation similar to ductile-dimple fracture mode, but the surfaces of the pores indicated granular features. Fracture surfaces of specimens deformed below the superplastic rates showed approximately 20 μm pore spacing (Figs 5a, b). A similar spacing of large cavities was also observed near the fracture surface in the optical micrographs, as seen in Fig. 1b. This mixed mode fracture consists of grain-boundary separation, as in superplastic fracture, where the necks that strain preferentially between cavities deform at superplastic rates. At the bottom of the cavities, the individual grain surfaces are still seen, so even though cavities appear round, they have the surface features of the grains that border them. Thus fracture does not result explicitly from the plasticity controlled manner observed in larger grain-size metals, but rather by a mixture of intergranular separation followed by the overall growth of cavities from vacancy flux along grain boundaries. These observations are consistent with the superplastic cavitation model of Chokshi and Langdon [17].

Intergranular fracture of superplastically deformed specimens is indicative of the grain-boundary sliding process that accounts for the sliding on the specimen surface and the large elongations (Fig. 5c). Intergranular failure predominates in the high-temperature deformation of IN9021. Cavity spacing, when it can be identified, is of the order of the 2 to 3 μm grain size. The conditions for increasing intergranular character of failure follow directly from optimizing conditions for grain-boundary sliding, which corresponds with optimum superplastic conditions.

At yet higher rates above the superplastic regime, the fracture surface again appears as a mixed mode of intergranular and ductile-dimple topography, but with 2 to 3 μm pore spacing (Fig. 5d). In this case the grain-boundary sliding process is no longer dominant, so cavities form of the order of the spacing between the grains. The conditions for increasing ductile failure phenomena are increasing strain rate above the optimum superplastic conditions, and decreasing temperature. Both of these conditions decrease the time available for grain-boundary dislocations to form from lattice dislocations. Consequently, the ability of grain-boundary dislocations and diffusion to accommodate the stress concentrations resulting from rapid dislocation arrival to the boundary is insufficient to maintain compatibility, and normal cavity growth leading to failure results.

The fracture surfaces described above differ from the observations of Shaw, who observed hair-like

whiskers on the fast-fracture part of the surface of a fracture specimen of IN9021 at 400° C [10]. The whiskers were approximately 0.5 μm diameter. Two features similar to Shaw's whiskers are evident in Fig. 4b. Because Shaw reported the grain size as submicrometre, he suggested that grain-boundary sliding could not account for the formation of the whiskers. He suggested that dynamic recrystallization could account for the whiskers, because a high flow stability would be possible. However, if the submicrometre grains recrystallized, then the smaller recrystallized grains could slide to permit the micro-superplasticity observed. Dynamic recrystallization can be beneficial for superplastic deformation, as an initially worked structure with lots of small-angle boundaries can be converted to smaller grains with more high-angle grain boundaries, which slide more effectively. This has been demonstrated in an Al–Li alloy, where an initial high strain rate causes dynamic recrystallization that provides an optimum small grain size for subsequent (lower strain rate) superplastic deformation [18].

Although no recrystallized grains were observed in TEM of specimens deformed to strains up to 0.5 (specimens became too small to easily make TEM specimens), recrystallization at larger strains seems unlikely due to the stability of the microstructure. Hawk and Wilsdorf observed no change in grain size after exposures to elevated temperature of over 0.4×10^6 sec at similar temperatures [19]. No apparent change in grain size was observed in the specimen shown in Fig. 3, which was deformed under 10 MPa at 475° C for 2.7×10^6 sec. An alternate explanation for the fibres in Shaw's fracture surface could be that the 2 to 3 μm subgrain clusters elongated by means of slip within the grain, with the low-angle boundaries remaining intact, and the high-angle boundaries becoming the surfaces of the fibres. Because the specimen orientation and strain rate of Shaw's result is unknown, this interpretation remains speculative.

4. Conclusions

Cavitation in superplastically deformed IN90211 is low, due to the accommodation of stress concentrations by slip in the grains during grain-boundary sliding. The orientation of high-angle grain boundaries parallel with the tensile axis and low-angle boundaries perpendicular to the tensile axis provides the minimal arrangement boundaries where cavities can easily grow in a tensile state of stress. This microstructural configuration resulted from extrusion and rolling texture. The inverted hour-glass appearance of the grain-boundary sliding can occur as a result of the sliding of platelet-shaped grains, and does not imply that a core–mantle deformation mechanism is necessarily operative. Superplastic elongations were obtained in an alloy that did not have equiaxed grains, so equiaxed grains are not a necessary condition for superplasticity. Finally, the use of hydrostatic pressure to minimize cavitation is unnecessary for superplasticity in IN9021(1), because grain-boundary sliding is not the rate-limiting process for superplastic deformation.

Acknowledgements

This work has been supported by the Air Force Office of Scientific Research under contract number AFOSR-86-0091. Additional support and the material was provided by the Research and Development Division of Lockheed Missiles and Space Co., Inc., where J. Wadsworth and T. G. Nieh also provided helpful discussions and some of the SEM work. X-ray diffraction data were obtained courtesy of Professor R. Shelton and T. Folkerts of the Physics Department at the University of California, Davis.

References

1. B. A. WILCOX and A. H. CLAUER, *Acta Metall.* **20** (1972) 743.
2. J. J. STEPHENS and W. D. NIX, *Metall. Trans.* **16A** (1985) 1307.
3. B. P. KASHYAP and A. K. MUKHERJEE, *Res Mech.* **17** (1986) 293.
4. J. E. FRANKLIN, J. MUKHOPADHYAY and A. K. MUKHERJEE, *Scripta Metall.* **22** (1988) 865.
5. J. PILLING and N. RIDLEY, *Acta Metall.* **34** (1986) 669.
6. W. C. OLIVER and W. D. NIX, *ibid.* **30** (1982) 1335.
7. J. S. BENJAMIN and M. J. BOMFORD, *Metall. Trans.* **8A** (1977) 1301.
8. T. G. NIEH, P. S. GILMAN and J. WADSWORTH, *Scripta Metall.* **19** (1985) 1375.
9. K. KUCHAROVA, A. ORLOVA, H. OIKAWA and J. CADEK, *Mater. Sci. Eng.* **A102** (1988) 201.
10. W. J. D. SHAW, *Mater. Lett.* **4** (1985) 1.
11. S. J. BANE, J. BRADFIELD and M. R. EDWARDS, *Mater. Sci. Tech.* **2** (1986) 1025.
12. T. R. BIELER, PhD dissertation, University of California at Davis, (1989) University Microfilms, Ann Arbor, Michigan.
13. T. R. BIELER, T. G. NIEH, J. WADSWORTH and A. K. MUKHERJEE, *Scripta Metall.* **22** (1988) 81.
14. M. OTSUKA, Y. ABE and R. HORIUCHI, in "Creep and Fracture of Engineering Materials and Structures", edited by B. Wilshire and R. W. Evans (The Institute of Metals, London, 1987) p. 307.
15. M. L. MAYO and W. D. NIX, *Acta Metall.* **37** (1989) 1121.
16. C. J. TWEED, B. RALPH and N. HANSEN, *ibid.* **32** (1984) 1407.
17. A. H. CHOKSHI and T. G. LANGDON, *Acta Metall.* **35** (1987) 1089.
18. B. A. ASH and C. H. HAMILTON, *Scripta Metall.* **22** (1988) 277.
19. J. A. HAWK and H. G. F. WILSDORF, *ibid.* **22** (1988) 561.

Received 11 July
and accepted 17 August 1989